DESY-97-060

Measurement of Elastic J/ψ Photoproduction at HERA

ZEUS Collaboration

Abstract

The reaction $\gamma\ p \to J/\psi\ p$ has been studied in ep interactions using the ZEUS detector at HERA. The cross section for elastic J/ψ photoproduction has been measured as a function of the photon-proton centre of mass energy W in the range $40 < W < 140$ GeV at a median photon virtuality Q^2 of 5×10^{-5} GeV^2. The photoproduction cross section, $\sigma_{\gamma p \to J/\psi p}$, is observed to rise steeply with W. A fit to the data presented in this paper to determine the parameter δ in the form $\sigma_{\gamma p \to J/\psi p} \propto W^{\delta}$ yields the value $\delta = 0.92 \pm 0.14 \pm 0.10$. The differential cross section $d\sigma/d|t|$ is presented over the range $|t| < 1.0$ GeV^2 where t is the square of the four-momentum exchanged at the proton vertex. $d\sigma/d|t|$ falls exponentially with a slope parameter of $4.6 \pm 0.4^{+0.4}_{-0.6}$ GeV^{-2}. The measured decay angular distributions are consistent with s-channel helicity conservation.

The ZEUS Collaboration

J. Breitweg, M. Derrick, D. Krakauer, S. Magill, D. Mikunas, B. Musgrave, J. Repond, R. Stanek, R.L. Talaga, R. Yoshida, H. Zhang
Argonne National Laboratory, Argonne, IL, USA [p]

M.C.K. Mattingly
Andrews University, Berrien Springs, MI, USA

F. Anselmo, P. Antonioli, G. Bari, M. Basile, L. Bellagamba, D. Boscherini, A. Bruni, G. Bruni, G. Cara Romeo, G. Castellini[1], L. Cifarelli[2], F. Cindolo, A. Contin, M. Corradi, S. De Pasquale, I. Gialas[3], P. Giusti, G. Iacobucci, G. Laurenti, G. Levi, A. Margotti, T. Massam, R. Nania, F. Palmonari, A. Pesci, A. Polini, G. Sartorelli, Y. Zamora Garcia[4], A. Zichichi
University and INFN Bologna, Bologna, Italy [f]

C. Amelung, A. Bornheim, I. Brock, K. Coböken, J. Crittenden, R. Deffner, M. Eckert, L. Feld[5], M. Grothe, H. Hartmann, K. Heinloth, L. Heinz, E. Hilger, H.-P. Jakob, U.F. Katz, E. Paul, M. Pfeiffer, Ch. Rembser, J. Stamm, R. Wedemeyer[6]
Physikalisches Institut der Universität Bonn, Bonn, Germany [c]

D.S. Bailey, S. Campbell-Robson, W.N. Cottingham, B. Foster, R. Hall-Wilton, M.E. Hayes, G.P. Heath, H.F. Heath, D. Piccioni, D.G. Roff, R.J. Tapper
H.H. Wills Physics Laboratory, University of Bristol, Bristol, U.K. [o]

M. Arneodo[7], R. Ayad, M. Capua, A. Garfagnini, L. Iannotti, M. Schioppa, G. Susinno
Calabria University, Physics Dept.and INFN, Cosenza, Italy [f]

J.Y. Kim, J.H. Lee, I.T. Lim, M.Y. Pac[8]
Chonnam National University, Kwangju, Korea [h]

A. Caldwell[9], N. Cartiglia, Z. Jing, W. Liu, J.A. Parsons, S. Ritz[10], S. Sampson, F. Sciulli, P.B. Straub, Q. Zhu
Columbia University, Nevis Labs., Irvington on Hudson, N.Y., USA [q]

P. Borzemski, J. Chwastowski, A. Eskreys, Z. Jakubowski, M.B. Przybycień, M. Zachara, L. Zawiejski
Inst. of Nuclear Physics, Cracow, Poland [j]

L. Adamczyk, B. Bednarek, K. Jeleń, D. Kisielewska, T. Kowalski, M. Przybycień, E. Rulikowska-Zarębska, L. Suszycki, J. Zając
Faculty of Physics and Nuclear Techniques, Academy of Mining and Metallurgy, Cracow, Poland [j]

Z. Duliński, A. Kotański
Jagellonian Univ., Dept. of Physics, Cracow, Poland [k]

G. Abbiendi[11], L.A.T. Bauerdick, U. Behrens, H. Beier, J.K. Bienlein, G. Cases[12], O. Deppe, K. Desler, G. Drews, U. Fricke, D.J. Gilkinson, C. Glasman, P. Göttlicher, J. Große-Knetter, T. Haas, W. Hain, D. Hasell, H. Heßling, K.F. Johnson[13], M. Kasemann, W. Koch, U. Kötz, H. Kowalski, J. Labs,
L. Lindemann, B. Löhr, M. Löwe[14], J. Mainusch[15], O. Mańczak, J. Milewski, T. Monteiro[16], J.S.T. Ng[17], D. Notz, K. Ohrenberg[15], I.H. Park[18], A. Pellegrino, F. Pelucchi, K. Piotrzkowski, M. Roco[19], M. Rohde, J. Roldán, J.J. Ryan, A.A. Savin, U. Schneekloth, W. Schulz[20], F. Selonke, B. Surrow, E. Tassi, T. Voß[21], D. Westphal, G. Wolf, U. Wollmer[22], C. Youngman, A.F. Żarnecki, W. Zeuner
Deutsches Elektronen-Synchrotron DESY, Hamburg, Germany

B.D. Burow, H.J. Grabosch, A. Meyer, S. Schlenstedt
DESY-IfH Zeuthen, Zeuthen, Germany

G. Barbagli, E. Gallo, P. Pelfer
University and INFN, Florence, Italy [f]

G. Maccarrone, L. Votano
INFN, Laboratori Nazionali di Frascati, Frascati, Italy [f]

A. Bamberger, S. Eisenhardt, P. Markun, T. Trefzger[23], S. Wölfle
Fakultät für Physik der Universität Freiburg i.Br., Freiburg i.Br., Germany [c]

J.T. Bromley, N.H. Brook, P.J. Bussey, A.T. Doyle, D.H. Saxon, L.E. Sinclair, E. Strickland, M.L. Utley[24], R. Waugh, A.S. Wilson
Dept. of Physics and Astronomy, University of Glasgow, Glasgow, U.K. [o]

I. Bohnet, N. Gendner, U. Holm, A. Meyer-Larsen, H. Salehi, K. Wick
Hamburg University, I. Institute of Exp. Physics, Hamburg, Germany [c]

L.K. Gladilin[25], R. Klanner, E. Lohrmann, G. Poelz, W. Schott[26], F. Zetsche
Hamburg University, II. Institute of Exp. Physics, Hamburg, Germany [c]

T.C. Bacon, I. Butterworth, J.E. Cole, V.L. Harris, G. Howell, B.H.Y. Hung, L. Lamberti[27], K.R. Long, D.B. Miller, N. Pavel, A. Prinias[28], J.K. Sedgbeer, D. Sideris, A.F. Whitfield[29]
Imperial College London, High Energy Nuclear Physics Group, London, U.K. [o]

U. Mallik, S.M. Wang, J.T. Wu
University of Iowa, Physics and Astronomy Dept., Iowa City, USA [p]

P. Cloth, D. Filges
Forschungszentrum Jülich, Institut für Kernphysik, Jülich, Germany

J.I. Fleck[30], T. Ishii, M. Kuze, M. Nakao, K. Tokushuku, S. Yamada, Y. Yamazaki[31]
Institute of Particle and Nuclear Studies, KEK, Tsukuba, Japan [g]

S.H. An, S.B. Lee, S.W. Nam, H.S. Park, S.K. Park
Korea University, Seoul, Korea [h]

F. Barreiro, J.P. Fernandez, R. Graciani, J.M. Hernández, L. Hervás, L. Labarga, M. Martinez, J. del Peso, J. Puga, J. Terron, J.F. de Trocóniz
Univer. Autónoma Madrid, Depto de Física Teóríca, Madrid, Spain [n]

F. Corriveau, D.S. Hanna, J. Hartmann, L.W. Hung, J.N. Lim, W.N. Murray, A. Ochs, M. Riveline, D.G. Stairs, M. St-Laurent, R. Ullmann
McGill University, Dept. of Physics, Montréal, Québec, Canada [a], [b]

T. Tsurugai
Meiji Gakuin University, Faculty of General Education, Yokohama, Japan

V. Bashkirov, B.A. Dolgoshein, A. Stifutkin
Moscow Engineering Physics Institute, Mosocw, Russia [l]

G.L. Bashindzhagyan, P.F. Ermolov, Yu.A. Golubkov, L.A. Khein, N.A. Korotkova, I.A. Korzhavina, V.A. Kuzmin, O.Yu. Lukina, A.S. Proskuryakov, L.M. Shcheglova, A.V. Shumilin,
A.N. Solomin, S.A. Zotkin
Moscow State University, Institute of Nuclear Physics, Moscow, Russia [m]

C. Bokel, M. Botje, N. Brümmer, F. Chlebana[19], J. Engelen, P. Kooijman, A. Kruse, A. van Sighem, H. Tiecke, W. Verkerke, J. Vossebeld, M. Vreeswijk, L. Wiggers, E. de Wolf
NIKHEF and University of Amsterdam, Netherlands [i]

D. Acosta, B. Bylsma, L.S. Durkin, J. Gilmore, C.M. Ginsburg, C.L. Kim, T.Y. Ling, P. Nylander, T.A. Romanowski[32]
Ohio State University, Physics Department, Columbus, Ohio, USA [p]

H.E. Blaikley, R.J. Cashmore, A.M. Cooper-Sarkar, R.C.E. Devenish, J.K. Edmonds, N. Harnew,
M. Lancaster[33], J.D. McFall, C. Nath, V.A. Noyes[28], A. Quadt, J.R. Tickner, H. Uijterwaal, R. Walczak,
D.S. Waters, T. Yip
Department of Physics, University of Oxford, Oxford, U.K. [o]

A. Bertolin, R. Brugnera, R. Carlin, F. Dal Corso, M. De Giorgi, U. Dosselli, S. Limentani, M. Morandin, M. Posocco, L. Stanco, R. Stroili, C. Voci, F. Zuin
Dipartimento di Fisica dell' Universita and INFN, Padova, Italy [f]

J. Bulmahn, R.G. Feild[34], B.Y. Oh, J.R. Okrasiński, J.J. Whitmore
Pennsylvania State University, Dept. of Physics, University Park, PA, USA [q]

Y. Iga
Polytechnic University, Sagamihara, Japan [g]

G. D'Agostini, G. Marini, A. Nigro, M. Raso
Dipartimento di Fisica, Univ. 'La Sapienza' and INFN, Rome, Italy [f]

J.C. Hart, N.A. McCubbin, T.P. Shah
Rutherford Appleton Laboratory, Chilton, Didcot, Oxon, U.K. [o]

E. Barberis[33], T. Dubbs, C. Heusch, M. Van Hook, W. Lockman, J.T. Rahn, H.F.-W. Sadrozinski,
A. Seiden, D.C. Williams
University of California, Santa Cruz, CA, USA [p]

O. Schwarzer, A.H. Walenta
Fachbereich Physik der Universität-Gesamthochschule Siegen, Germany [c]

H. Abramowicz, G. Briskin, S. Dagan[35], T. Doeker, S. Kananov, A. Levy[36]
Raymond and Beverly Sackler Faculty of Exact Sciences, School of Physics, Tel-Aviv University,
Tel-Aviv, Israel [e]

T. Abe, M. Inuzuka, K. Nagano, I. Suzuki, K. Umemori
Department of Physics, University of Tokyo, Tokyo, Japan [g]

R. Hamatsu, T. Hirose, K. Homma, S. Kitamura[37], T. Matsushita, K. Yamauchi
Tokyo Metropolitan University, Dept. of Physics, Tokyo, Japan [g]

R. Cirio, M. Costa, M.I. Ferrero, S. Maselli, V. Monaco, C. Peroni, M.C. Petrucci, R. Sacchi, A. Solano, A. Staiano
Universita di Torino, Dipartimento di Fisica Sperimentale and INFN, Torino, Italy [f]

M. Dardo
II Faculty of Sciences, Torino University and INFN - Alessandria, Italy [f]

D.C. Bailey, M. Brkic, C.-P. Fagerstroem, G.F. Hartner, K.K. Joo, G.M. Levman, J.F. Martin, R.S. Orr, S. Polenz, C.R. Sampson, D. Simmons, R.J. Teuscher[30]
University of Toronto, Dept. of Physics, Toronto, Ont., Canada [a]

J.M. Butterworth, C.D. Catterall, T.W. Jones, P.B. Kaziewicz, J.B. Lane, R.L. Saunders, J. Shulman, M.R. Sutton
University College London, Physics and Astronomy Dept., London, U.K. [o]

B. Lu, L.W. Mo
Virginia Polytechnic Inst. and State University, Physics Dept., Blacksburg, VA, USA [q]

J. Ciborowski, G. Grzelak[38], M. Kasprzak, K. Muchorowski[39], R.J. Nowak, J.M. Pawlak, R. Pawlak, T. Tymieniecka, A.K. Wróblewski, J.A. Zakrzewski
Warsaw University, Institute of Experimental Physics, Warsaw, Poland [j]

M. Adamus
Institute for Nuclear Studies, Warsaw, Poland [j]

C. Coldewey, Y. Eisenberg[35], D. Hochman, U. Karshon[35], D. Revel[35]
Weizmann Institute, Nuclear Physics Dept., Rehovot, Israel [d]

W.F. Badgett, D. Chapin, R. Cross, S. Dasu, C. Foudas, R.J. Loveless, S. Mattingly, D.D. Reeder, W.H. Smith, A. Vaiciulis, M. Wodarczyk
University of Wisconsin, Dept. of Physics, Madison, WI, USA [p]

S. Bhadra, W.R. Frisken, M. Khakzad, W.B. Schmidke
York University, Dept. of Physics, North York, Ont., Canada [a]

[1] also at IROE Florence, Italy
[2] now at Univ. of Salerno and INFN Napoli, Italy
[3] now at Univ. of Crete, Greece
[4] supported by Worldlab, Lausanne, Switzerland
[5] now OPAL
[6] retired
[7] also at University of Torino and Alexander von Humboldt Fellow
[8] now at Dongshin University, Naju, Korea
[9] also at DESY and Alexander von Humboldt Fellow
[10] Alfred P. Sloan Foundation Fellow
[11] supported by an EC fellowship number ERBFMBICT 950172
[12] now at SAP A.G., Walldorf
[13] visitor from Florida State University
[14] now at ALCATEL Mobile Communication GmbH, Stuttgart
[15] now at DESY Computer Center
[16] supported by European Community Program PRAXIS XXI
[17] now at DESY-Group FDET
[18] visitor from Kyungpook National University, Taegu, Korea, partially supported by DESY
[19] now at Fermi National Accelerator Laboratory (FNAL), Batavia, IL, USA
[20] now at Siemens A.G., Munich
[21] now at NORCOM Infosystems, Hamburg
[22] now at Oxford University, supported by DAAD fellowship HSP II-AUFE III
[23] now at ATLAS Collaboration, Univ. of Munich
[24] now at Clinical Operational Research Unit, University College, London
[25] on leave from MSU, supported by the GIF, contract I-0444-176.07/95
[26] now a self-employed consultant
[27] supported by an EC fellowship
[28] PPARC Post-doctoral Fellow
[29] now at Conduit Communications Ltd., London, U.K.
[30] now at CERN
[31] supported by JSPS Postdoctoral Fellowships for Research Abroad
[32] now at Department of Energy, Washington
[33] now at Lawrence Berkeley Laboratory, Berkeley
[34] now at Yale University, New Haven, CT
[35] supported by a MINERVA Fellowship
[36] partially supported by DESY
[37] present address: Tokyo Metropolitan College of Allied Medical Sciences, Tokyo 116, Japan
[38] supported by the Polish State Committee for Scientific Research, grant No. 2P03B09308
[39] supported by the Polish State Committee for Scientific Research, grant No. 2P03B09208

[a] supported by the Natural Sciences and Engineering Research Council of Canada (NSERC)
[b] supported by the FCAR of Québec, Canada
[c] supported by the German Federal Ministry for Education and Science, Research and Technology (BMBF), under contract numbers 057BN19P, 057FR19P, 057HH19P, 057HH29P, 057SI75I
[d] supported by the MINERVA Gesellschaft für Forschung GmbH, the German Israeli Foundation, and the U.S.-Israel Binational Science Foundation
[e] supported by the German Israeli Foundation, and by the Israel Science Foundation
[f] supported by the Italian National Institute for Nuclear Physics (INFN)
[g] supported by the Japanese Ministry of Education, Science and Culture (the Monbusho) and its grants for Scientific Research
[h] supported by the Korean Ministry of Education and Korea Science and Engineering Foundation
[i] supported by the Netherlands Foundation for Research on Matter (FOM)
[j] supported by the Polish State Committee for Scientific Research, grant No. 115/E-343/SPUB/P03/120/96
[k] supported by the Polish State Committee for Scientific Research (grant No. 2 P03B 083 08) and Foundation for Polish-German Collaboration
[l] partially supported by the German Federal Ministry for Education and Science, Research and Technology (BMBF)
[m] supported by the German Federal Ministry for Education and Science, Research and Technology (BMBF), and the Fund of Fundamental Research of Russian Ministry of Science and Education and by INTAS-Grant No. 93-63
[n] supported by the Spanish Ministry of Education and Science through funds provided by CICYT
[o] supported by the Particle Physics and Astronomy Research Council
[p] supported by the US Department of Energy
[q] supported by the US National Science Foundation

1 Introduction

This paper reports new data on the photoproduction of the J/ψ meson using the ZEUS detector at HERA. It is part of our continuing study of vector meson ($\rho, \omega, \phi, J/\psi$) production in both the photoproduction [1, 2, 3, 4] and the deep inelastic scattering regimes [5, 6]. Previous results have established a weak dependence on the photon-proton centre of mass energy, W, of the vector meson photoproduction cross sections ($\sigma \propto W^{\delta}$ with $\delta \sim 0.2 - 0.3$) if there is no hard scale in the process, as expected from soft diffraction. By contrast, the cross sections for elastic ρ and ϕ production in deep inelastic scattering at $5 \lesssim Q^2 \lesssim 20$ GeV^2 exhibit a stronger W dependence ($\sigma \propto W^{\delta}$ with $\delta \sim 0.3 - 0.6$) where Q^2 sets the hard scale. In the photoproduction of the J/ψ meson the mass of the J/ψ itself provides the hard scale and the cross section exhibits a strong W dependence ($\sigma \propto W^{\delta}$ with $\delta \sim 1$). The total virtual photon-proton cross section [7, 8] also exhibits a change in energy dependence as Q^2 increases beyond ≈ 1 GeV^2. Overall, the data illuminate the transition from the soft, non-perturbative regime to the kinematic region where perturbative descriptions become applicable.

J/ψ photoproduction has been measured as a function of W from threshold to $W \approx 20$ GeV in fixed target experiments [9, 10, 11] and extended to $W \approx 140$ GeV at HERA [4, 12, 13]. A review of the low energy experimental results can be found in reference [14]. In this paper we extend our earlier study of elastic J/ψ photoproduction [4] to include the determination of the differential cross section $d\sigma/d|t|$ and the angular distributions of the decay leptons. In addition, the six-fold increase in the size of the data sample allows us to determine the parameter δ from the data presented here alone.

The J/ψ was detected via its leptonic (electron pair and muon pair) decay modes in the kinematic range $40 < W < 140$ GeV. After a brief description of the ZEUS detector, the data taking conditions, the kinematics of elastic J/ψ production at HERA, and the event selection are described. The W dependence of the cross section $\sigma_{\gamma p \to J/\psi p}$, the t distribution and the decay angular distributions are then presented.

2 Experimental Conditions

2.1 HERA

During 1994 HERA operated with a proton beam energy of 820 GeV and a positron beam energy of 27.5 GeV. In the positron and proton beams 153 colliding bunches were stored together with 17 unpaired proton bunches and 15 unpaired positron bunches. The time between bunch crossings was 96 ns. The typical instantaneous luminosity was 1.5×10^{30} cm^{-2} s^{-1}.

2.2 The ZEUS Detector

The main ZEUS detector components used in this analysis are outlined below. A detailed description of the ZEUS detector can be found elsewhere [15]. In the following the ZEUS

coordinate system will be used, the Z axis of which is coincident with the nominal proton beam axis, the X axis is horizontal and points towards the centre of HERA and the Y axis completes a right handed coordinate system. The origin of the coordinate system lies at the nominal interaction point.

The momentum and trajectory of a charged particle were reconstructed using the Vertex Detector (VXD) [16] and the Central Tracking Detector (CTD) [17]. The VXD and the CTD are cylindrical drift chambers which are placed in the solenoidal magnetic field of 1.43 T produced by a thin superconducting solenoid. The CTD surrounds the VXD and covers the angular region $15^o < \theta < 164^o$ (where θ is the polar angle with respect to the proton direction).

The high resolution uranium-scintillator calorimeter CAL [18] surrounding the coil is divided into three parts, the forward calorimeter (FCAL), the barrel calorimeter (BCAL) and the rear calorimeter (RCAL), which cover polar angles from 2.6^o to 36.7^o, 36.7^o to 129.1^o, and 129.1^o to 176.2^o, respectively. Each part consists of towers which are longitudinally subdivided into electromagnetic (EMC) and hadronic (HAC) readout cells.

The proton remnant tagger (PRT), a set of scintillation counters surrounding the beam pipe at small forward angles, serves to tag events with proton dissociation. It is situated at $Z = 500$ cm and covers the angular range from 6 to 26 mrad.

The muon detectors [19], situated outside the calorimeter, consist of limited streamer tubes (LST) placed both inside and outside the magnetised iron yoke. The inner chambers (BMUI and RMUI) were used to tag the muons from the J/ψ. The BMUI and the RMUI cover the polar angles between $34^o < \theta < 135^o$ and $134^o < \theta < 171^o$, respectively.

Proton-gas events occuring upstream of the nominal interaction point are out of time with respect to the e^+p interactions and were rejected by timing measurements made by the scintillation counter arrays Veto Wall, C5 and SRTD situated along the beam line at $Z = -730$ cm, $Z = -315$ cm, and $Z = -150$ cm respectively.

The luminosity was determined from the rate of the Bethe-Heitler process $e^+p \to e^+\gamma p$ where the photon was measured by the LUMI calorimeter located in the HERA tunnel at $Z = -107$ m [20]. The luminosity was determined with a precision of 1.5% for the measurements presented below.

3 Kinematics

Figure 1a shows a schematic diagram for the reaction:

$$e^+(k)p(P) \to e^+(k')J/\psi(V)p(P'), \tag{1}$$

where each symbol in parentheses denotes the four-momentum of the corresponding particle.

The kinematics of the inclusive scattering of unpolarised positrons and protons are described by the positron-proton centre of mass energy squared (s) and any two of the following variables

- $Q^2 = -q^2 = -(k - k')^2$, the negative four-momentum squared of the exchanged photon;
- $y = (q \cdot P)/(k \cdot P)$, the fraction of the positron energy transferred to the hadronic final state in the rest frame of the initial state proton;
- $W^2 = (q + P)^2 = -Q^2 + 2y(k \cdot P) + M_p^2 \approx ys$, the centre of mass energy squared of the photon-proton system, where M_p is the proton mass.

For a complete description of the exclusive reaction $e^+p \to e^+J/\psi p$ ($J/\psi \to \ell^+\ell^-$, where $\ell^+\ell^-$ denotes a pair of electrons or muons) the following additional variables are required

- $t = (P - P')^2$, the four-momentum transfer squared at the proton vertex;
- the angle between the J/ψ production plane and the positron scattering plane in the photon-proton frame, Φ;
- the polar and azimuthal angles, θ_h and ϕ_h, of the decay leptons in the J/ψ rest frame.

In the present analysis, Φ is not measured because events were selected in which the scattered positron was not detected. In such untagged photoproduction events the Q^2 value ranges from the kinematic minimum $Q^2_{min} = M_e^2 y^2/(1 - y) \approx 10^{-10}$ GeV^2, where M_e is the electron mass, to the value at which the scattered positron starts to be observed in the uranium calorimeter $Q^2_{max} \approx 4$ GeV^2, with a median Q^2 of approximately 5×10^{-5} GeV^2. Since the typical Q^2 is small, the photon-proton centre of mass energy can be expressed as

$$W^2 \approx 2(E_{J/\psi} - p_{ZJ/\psi})E_p = 4E_pE_ey, \tag{2}$$

where E_p and $E_{J/\psi}$ are the laboratory energies of the incoming proton and the J/ψ and $p_{ZJ/\psi}$ is the longitudinal momentum of the J/ψ. The four-momentum transfer squared, t, at the proton vertex for $Q^2 = Q^2_{min}$ is given by

$$t = (q - V)^2 \approx -p^2_{TJ/\psi}, \tag{3}$$

where $p_{TJ/\psi}$ is the momentum of the J/ψ transverse to the beam axis. Non-zero values of Q^2 cause t to differ from $-p^2_{TJ/\psi}$ by less than Q^2. A correction is applied to the $p^2_{TJ/\psi}$ distribution to correct for this effect as described in section 9.3 [1].

4 Trigger

ZEUS uses a three-stage trigger system [15]. The electron and muon pair triggers are outlined below, followed by a summary of trigger requirements common to both channels.

Electron Channel

The First Level Trigger (FLT) required 1, 2 or 3 track segments to be found in the CTD, with at least one segment pointing to the interaction region. The sum of all the energy deposited in the EMC section of the calorimeter was required to exceed 0.66 GeV. In addition, either the total energy in the calorimeter had to be greater than 2 GeV or the total energy in FCAL (ignoring the cells closest to the beam pipe) had to be greater than 2.5 GeV.

The Second Level Trigger (SLT) required the total energy in the HAC section of the calorimeter to be less than 1 GeV and the total energy in the EMC section to be greater than 1.5 GeV. The ratio of HAC to EMC energy in RCAL and BCAL separately had to be less than 0.1 or the HAC energy had to be less than 0.2 GeV.

The Third Level Trigger (TLT) matched tracks measured in the CTD to electromagnetic energy deposits in the calorimeter. A cluster of contiguous cells, each with an energy of at least 0.3 GeV, was defined as electromagnetic if more than 90% of the total cluster energy was contained in EMC cells. An electron candidate was defined as a track with momentum transverse to the beam direction in excess of 0.4 GeV passing within 30 cm of the centre of an electromagnetic cluster. At least two electron candidates of opposite charge were required. At the distance of closest approach the separation between the two tracks was required to be less than 7 cm. An event was kept if the invariant mass of any pair exceeded 2 GeV.

Muon Channel

At the FLT, track segments had to be found in the inner barrel muon chambers (BMUI) accompanied by a reconstructed energy deposition of at least 0.464 GeV in a CAL trigger tower. Note that on average a muon produces a visible signal of 0.8 GeV in a trigger tower. Alternatively, hits had to be found in the RMUI chambers accompanied by a reconstructed energy deposit of at least 0.464 GeV in an RCAL trigger tower [15]. At least one and no more than five track segments had to be found in the CTD, with at least one pointing to the interaction region.

No requirements were imposed at the SLT.

At the TLT a muon candidate was formed when a track found in the CTD matched a cluster of energy in the calorimeter consistent with the passage of a minimum ionising particle (m.i.p.) and a track in the inner muon chambers. An event containing a muon candidate for which $\theta > 147^o$ was accepted if the momentum exceeded 1 GeV. The transverse momentum of a muon candidate for which $20^o < \theta < 147^o$ was required to exceed 1 GeV.

Common Requirements

An event was rejected at the FLT if the time of arrival of any signal observed in the Veto

Wall, the C5 counter or the SRTD was inconsistent with the time of the bunch crossing. In order to increase the purity of the sample the sum of energy in the inner ring of FCAL was required to be less than 1.25 GeV.

At the SLT, the total energy in the calorimeter ($E_{Tot} = \Sigma_i E_i$) and the Z component of the momentum ($\Sigma p_Z = \Sigma_i E_i \cos\theta_i$) was calculated. The sums run over all calorimeter cells i for which the energy, E_i, deposited in the cell is above threshold and the polar angle at which the cell is found is denoted by θ_i. Beam-gas events were rejected by exploiting the excellent time resolution of the calorimeter. In order to remove inclusive beam-gas background in time with the bunch crossing, an event was rejected if the ratio $\Sigma p_Z / E_{Tot}$ was greater than 0.96.

Finally, at the TLT, E_{Tot} and Σp_Z were calculated again using the CAL energies reconstructed at the TLT, and an event was accepted if $E_{Tot} - \Sigma p_Z \leq 100$ GeV and $\Sigma p_Z / E_{Tot} \leq 0.94$.

5 Offline Event Selection

To be accepted an event was required to have exactly two tracks of opposite charge with pseudorapidity, η, in the range $|\eta| < 1.7$. Denoting the polar angle of a track by θ, η is defined such that $\eta = -\ln(\tan(\theta/2))$. The two tracks were required to fit to a common vertex consistent with an ep interaction. The tracks had to match to clusters of energy in the calorimeter and events were rejected if more than 1 GeV was deposited in calorimeter cells not associated with either of the two tracks. As shown in equation (2), W^2 was determined from the measured $E_{J/\psi} - p_{ZJ/\psi}$ of the decay leptons. The requirement that the value of W lie in the range $40 < W < 140$ GeV restricted the sample to a region of high acceptance. Selection criteria specific to the electron and muon channel are described below.

Electron Channel

The electron sample comes from an integrated luminosity of 2.70 ± 0.04 pb^{-1}. The algorithm used to define the electron pair sample at the TLT was reapplied offline with the final detector calibrations. The transverse momentum threshold of each of the two oppositely charged tracks was increased to 0.8 GeV. In order to reduce contamination from misidentified pions, the energy of at least one of the electromagnetic clusters matched to the tracks by the TLT algorithm applied offline was required to be larger than 1 GeV.

Figure 2a shows the mass distribution of the electron pair sample. A clear peak at the J/ψ mass is observed. The signal region, $2.85 < M_{e^+e^-} < 3.25$ GeV, contains 392 events. The cross sections and angular distributions presented below are obtained by calculating acceptances and background contributions for this range. The solid line shows an unbinned likelihood fit in which a Gaussian resolution function has been convoluted with a radiative J/ψ mass spectrum and a polynomial describing the background. The mass estimated by the fit is 3.094 ± 0.003 GeV, the rms width is 33 ± 4 MeV, and the

number of events attributable to J/ψ production estimated by the fit over the mass range $2 < M_{e^+e^-} < 4$ GeV is 460 ± 25.

Muon Channel

The muon sample comes from an integrated luminosity of 1.87 ± 0.03 pb^{-1}. The momentum of each track was required to exceed 1 GeV. At least one of the two tracks had to match a m.i.p. cluster in the calorimeter and a track segment in the barrel or rear muon chambers. To remove cosmic ray contamination the calorimeter signals were required to be in time with the beam crossing and the distance between the two tracks must be less than 2 cm at their distance of closest approach to the beamline. To further reduce the cosmic ray background the tracks were required not to be collinear. This was achieved by calculating the cosine of the angle, Ω, between the two tracks at the interaction point. An event was rejected if $\cos\Omega < -0.99$.

The mass distribution for the events passing the muon pair selection is shown in figure 2b. A clear peak over a flat background is observed. The signal region, $2.95 < M_{\mu^+\mu^-} < 3.25$ GeV, contains 289 events. The cross sections and angular distributions presented below are obtained by calculating acceptances and background contributions for this range. An unbinned likelihood fit to the sum of a Gaussian signal plus a flat background gives a value of 3.086 ± 0.003 GeV for the mass, 38 ± 3 MeV for the rms width and 266 ± 17 for the number of events attributable to J/ψ production in the mass range $2 < M_{\mu^+\mu^-} < 4$ GeV.

6 Monte Carlo Simulation and Acceptance Calculation

The reaction $e^+\ p \to e^+\ J/\psi\ p$ (figure 1a) was modelled using the DIPSI Monte Carlo program [21]. This Monte Carlo is based on the model of Ryskin [22] in which it is assumed that the exchanged photon fluctuates into a $c\bar{c}$ pair which then interacts with a gluon ladder emitted by the incident proton. The events are generated with a cross section proportional to W^δ and with an exponential t distribution proportional to $exp(-b|t|)$. Good agreement between the generated and observed distributions is obtained for $\delta = 1$ and $b = 4$ GeV^{-2}. In order to determine the systematic error on the acceptance δ was varied in the range $0 < \delta < 2$. The acceptance was found to be insensitive to the variation of b in the range $3 < b < 5$ GeV^{-2}.

Events were generated in the W range $20 < W < 210$ GeV and between Q^2_{min} and $Q^2 = 4$ GeV^2. The centre of mass decay of the J/ψ was generated with a $(1 + \alpha \cos^2\theta_h)$ distribution with $\alpha = 1$. Varying the value of α from 1 to 0.4, corresponding to about one standard deviation variation around the measurement presented in section 9.4, the acceptance grows by less than 10%. A systematic error due to this uncertainty is included in the total systematic error as described in section 8. The effects of positron initial and final state radiation and that of vacuum polarisation loops were neglected; the effects on the integrated cross section have been estimated to be smaller than 4% [1].

The events were then passed through a detailed simulation of the ZEUS detector and trigger. Parameterisations of noise distributions obtained from data taken with a random trigger were used to simulate the calorimeter noise contribution to the energy measurements. The simulated events were subjected to the same reconstruction and analysis programs as the data. The distributions of the reconstructed kinematic quantities obtained using DIPSI are in good agreement with those from the data. The overall acceptance was obtained as the ratio of the number of accepted Monte Carlo events to the number generated in the selected kinematic range. The acceptance, calculated in this manner, accounts for the geometric acceptance, for the detector, trigger and reconstruction efficiencies, and for the detector resolution. Table 1 shows the acceptances in various W ranges determined for each decay mode.

7 Background

In addition to elastic J/ψ photoproduction, the following processes may contribute to the final sample:

- The Bethe-Heitler process in which a lepton pair is produced by the fusion of a photon radiated by the positron with a photon radiated by the proton. This process was simulated using the LPAIR Monte Carlo [23] which was used to generate events in which the proton remains intact ('elastic' events) and events in which the proton dissociates ('dissociative' events). The size of the Bethe-Heitler contribution to the non-resonant background is shown in figure 2 where the $\ell^+\ell^-$ mass distributions are plotted. The QED cross section [24] for the elastic and dissociative Bethe-Heitler processes have been used to determine the normalisation of the appropriate LPAIR Monte Carlo sample. Figure 2 shows that the Bethe-Heitler process saturates the non-resonant background in the muon channel and is the dominant source of non-resonant background in the electron channel. The calculated background due to the Bethe-Heitler process in the signal region is 38 ± 1 for the electron channel and 23 ± 1 for the muon channel.

- Pions misidentified as electrons in the electron sample. For e^+e^- masses larger than 2.5 GeV the Bethe-Heitler contribution saturates the non-resonant background. The residual contribution of misidentified pions in the final sample was shown to be less than 1.5% by studying the distribution of dE/dX obtained using the pulse height information from the CTD. No subtraction has been made for pion misidentification. A systematic error of -1.5% attributed to the uncertainty in the pion contamination was included in the final systematic error.

- J/ψ produced via the production and decay of ψ'. The only ψ' decay mode giving a significant contribution to the J/ψ signal is $\psi' \to J/\psi\pi^0\pi^0$.

- Proton dissociative J/ψ production (figure 1b). The EPSOFT Monte Carlo was used to simulate this process. EPSOFT is based on the assumption that the diffractive cross section is of the form $d\sigma/d|t|dM_N^2 \propto e^{-b_d|t|}/M_N^\beta$ where M_N is the mass of the dissociative system. The simulation of the hadronisation of the dissociative

system includes a parameterisation of the resonance spectrum. To cross-check the results the generator PYTHIA [25] was also used which contains a different parameterisation of the resonance spectrum.

After the subtraction of the Bethe-Heitler contribution, the production of J/ψ mesons via the decay of the ψ' and proton dissociative J/ψ production are the only significant sources of background and will be discussed separately below.

The ψ' contribution was determined using a sample of events in which the ψ' decayed to a muon pair (branching ratio $\mathcal{B}_1 = (0.77 \pm 0.17)\%$ [26]). This sample was obtained using the same cuts as those used to isolate the $J/\psi \to \mu^+\mu^-$ sample (see section 5). A signal of $N_1 = 7 \pm 4$ events was found at the ψ' mass in a sample for which the integrated luminosity, $\mathcal{L}_1$, was 2.70 ± 0.04 pb^{-1}. The corresponding acceptance, $\mathcal{A}_1$, computed with DIPSI, was $\mathcal{A}_1 = 0.35$. The number of events from ψ' production entering the elastic $J/\psi \to \mu^+\mu^-$ sample via the decay $\psi' \to J/\psi\pi^0\pi^0$ was estimated using the formula

$$N_C = \frac{N_1}{\mathcal{A}_1\ \mathcal{L}_1\ \mathcal{B}_1}\mathcal{A}_C^{\mu}\mathcal{L}_C\mathcal{B}_C\mathcal{B}, \tag{4}$$

where $\mathcal{B} = (6.01 \pm 0.19)\%$ is the branching ratio for the decay $J/\psi \to \mu^+\mu^-$, $\mathcal{B}_C$ is that for the decay $\psi^{'} \to \psi\pi^0\pi^0$ ($\mathcal{B}_C = (18.4 \pm 2.7)\%$) [26], $\mathcal{L}_C$ is the luminosity from which the muon sample defined in section 5 was drawn ($\mathcal{L}_C = 1.9$ pb^{-1}) and $\mathcal{A}_C^{\mu}$ is the acceptance for the process $e^+p \to e^+\psi' p$ ($\psi' \to \mu^+\mu^-\pi^0\pi^0$), using DIPSI $\mathcal{A}_C^{\mu} = 0.28$. The formula (4) leads to a ψ' contamination of $(2.3 \pm 1.4)\%$. This result was cross-checked by selecting events in which the ψ' decayed into $\mu^+\mu^-\pi^+\pi^-$. In this case 7 ± 3 events were found at the ψ' mass and a contamination of $(3.4 \pm 1.4)\%$ was estimated. The two results may be combined to give a final estimate of the ψ' contamination of $(3 \pm 1)\%$. This contamination was subtracted from both the electron and muon sample.

The proton dissociative process is characterised by a cross section of the form

$$\frac{d\sigma}{d|t|dM_N^2} \propto \frac{e^{-b_d|t|}}{M_N^{\beta}}. \tag{5}$$

In order to estimate the value of b_d, dissociative events were selected in which the J/ψ was accompanied by an energy deposit in the inner ring of FCAL or in the PRT. The value $b_d = 1$ GeV^{-2} was found to give the best description of the $p_{TJ/\psi}$ distribution of the PRT tagged sample. The systematic error in the dissociative contribution caused by the uncertainty in b_d was estimated by varying b_d in the range $0.4 < b_d < 2$ GeV^{-2}. This assumption is consistent with the result $b_d = 1.6 \pm 0.3 \pm 0.1$ GeV^{-2} reported by the H1 collaboration[13]. The value $\beta = 2.25$ was used as the central value in the simulation of the M_N distribution and β varied in the range $2 < \beta < 2.5$ to estimate the systematic error. This assumption is consistent with the result $\beta = 2.20 \pm 0.03$ recently obtained at Fermilab for the diffractive dissociation of the proton in $\bar{p}p$ collisions [27]. The mass of the nucleonic system was generated in the range $(1.25\ \text{GeV}^2) \leq M_N^2 \leq 0.1\ W^2$.

The proton dissociative contribution to the electron sample was determined by selecting a sample, D_e, for which the requirement that $E_{Tot} - E_{J/\psi} < 1$ GeV was replaced by the

three cuts $E_F > 1$ GeV, $E_B < 1$ GeV and $E_R < 1$ GeV. E_F, E_B and E_R were calculated by summing the energy in the FCAL, BCAL and RCAL respectively. The calorimeter cells associated with the electron candidates were excluded from these sums. The cut on E_F selects dissociative events in which energy is deposited in the proton direction, while the cut on E_R ensures that events in which the scattered positron is detected in RCAL do not enter the sample. The cut on E_B ensures that inelastic events depositing energy in BCAL also do not enter the sample. The proton dissociative sample, D_e, was further examined by studying the distribution of the energy weighted pseudorapidity defined by

$$\bar{\eta}_C = \frac{\Sigma_i E_i \eta_i}{\Sigma_i E_i}, \tag{6}$$

where E_i is the energy of a calorimeter cell and η_i is the pseudorapidity of the cell and the sum runs over all cells containing more than 200 MeV but excluding those matched to the tracks forming the J/ψ candidate. The distribution of $\bar{\eta}_C$ for dissociative events, simulated using the EPSOFT Monte Carlo, is strongly peaked at $\bar{\eta}_C > 2$. In the sample D_e there are 2 events for which $\bar{\eta}_C > 2$. The ratio of the number of EPSOFT events passing the elastic cuts to the number with $E_F > 1$ GeV, $E_B < 1$ GeV, $E_R < 1$ GeV and $\bar{\eta}_C > 2$ was 58. This leads to a dissociative contribution to the elastic J/ψ to electron sample of $(33^{+43+7+\ 0}_{-12-6-18})\%$. The first error is statistical and the second error is the systematic error resulting from the allowed variation of β in the Monte Carlo generation of dissociative events. When the calculation is repeated with EPSOFT replaced by PYTHIA the result differs by -18% from that reported above. The third error quoted in the dissociative contribution reflects this uncertainty in the simulation of the dissociative final state. The change in the dissociative contribution obtained when b_d was varied in the range $0.4 < b_d < 2$ GeV^{-2} was found to be negligible.

The same procedure was applied to the muon sample with the only difference that the cut on $\bar{\eta}_C$ was not applied. The proton dissociative sample obtained contained 7 events and the ratio of the number of EPSOFT events passing the elastic cuts to the number with $E_F > 1$ GeV, $E_B < 1$ GeV, $E_R < 1$ GeV was 11. This leads to a dissociative contribution of $(29 \pm 11^{+6\ +\ 0}_{-5\ -10})\%$.

Independent estimates of the dissociative contribution were made using dissociative events tagged by the PRT. EPSOFT was used to estimate the fraction of untagged dissociative events in the elastic sample since it was found that PYTHIA gives a poor description of the multiplicity distribution observed in the PRT. The dissociative contamination estimated in this way was $(34 \pm 8)\%$ for the electron channel and $(27 \pm 8)\%$ for the muon channel. The errors quoted are statistical only.

The four independent results were combined to give a final estimate of the dissociative contribution of $(30 \pm 5^{+7\ +\ 0}_{-6\ -10})\%$.

8 Systematic Errors

Several factors contribute to the systematic errors in the elastic J/ψ cross section measurement. In the following they are divided in two categories: *decay channel specific errors*

and *common systematic errors*. The first category contains systematic errors specific to the electron or muon decay channel, while the second contains systematic errors common to both decay channels. Table 2 summarises all these systematic errors.

Decay channel specific errors:

- *Trigger*: For the electron channel, the dominant systematic error due to the FLT acceptance is given by the requirement $E_{Tot} > 2$ GeV. At the SLT the dominant systematic error is contributed by the simulation of the calorimeter noise. For the muon channel, the dominant systematic error is contributed by the uncertainties in the simulation of the trigger threshold and the CTD-FLT track reconstruction. No systematic error in either channel is attributed to the TLT acceptance since all cuts are superseded by more stringent requirements offline.

- *Event selection*: In this class we include the systematic errors due to uncertainties in the measurement of momentum, transverse momentum, $|\eta|$ and the choice of the mass window. For the electron channel uncertainties in the cuts used to define an electron cluster also contribute. For the muon channel this class also contains the uncertainties coming from the collinearity cut. Each cut was varied within a range determined by the resolution of the quantity in question and the changes induced in the results were taken as an estimate of the corresponding systematic error. The different systematic errors were summed in quadrature.

- *Pion misidentification*: This class applies to the electron channel only; the method used to determine the systematic error was described in section 7.

- *Muon chamber efficiency*: The systematic error attributed to errors in the muon chamber reconstruction efficiency was estimated by using cosmic ray events.

- *Branching ratio*: The error on the branching ratio $J/\psi \to \ell^+\ell^-$ as quoted in [26].

Common systematic errors:

- *Acceptance*: The uncertainty in the acceptance was estimated by varying the parameters b and δ as described in section 6.

- *Elastic definition*: The systematic uncertainty contributed by the criterion used to classify an event as elastic was estimated by changing the elastic definition: $E_{Tot} - E_{J/\psi} < 1$ GeV to $E_{Tot} - E_{J/\psi} < 0.7$ GeV and to $E_{Tot} - E_{J/\psi} < 1.3$ GeV.

- *Radiative corrections*: The effects of positron initial and final state radiation and that of vacuum polarisation loops were neglected; the effects on the integrated cross section have been estimated to be smaller than 4% [1]. We take 4% as an estimate of the systematic error attributable to this source.

- *Helicity distribution:* The centre of mass decay of the J/ψ was generated with a $(1 + \alpha \cos^2 \theta_h)$ distribution. The systematic error was evaluated by varying the value of α from 1 to 0.4.

- *M_N distribution in proton dissociation*: As explained in section 7 this is obtained by changing the parameter β in the range $2 \leq \beta \leq 2.5$.
- *Model of dissociation:* The dependence on the modelling of the hadronic final state in proton dissociation was obtained by comparing the contamination obtained using PYTHIA with that obtained using EPSOFT (see section 7).
- *ψ' contamination*: As explained in section 7 the systematic error on the ψ' contribution is 1%.
- *Luminosity*: As indicated in section 2.2 the uncertainty of the luminosity determination is 1.5%.

9 Results

9.1 Integrated Cross Sections

The cross section for elastic J/ψ electroproduction is given by

$$\sigma_{ep\to eJ/\psi p} = \frac{N_{Evt}}{\mathcal{L}\mathcal{A}\mathcal{B}}, \tag{7}$$

where $\mathcal{L}$ is the integrated luminosity, $\mathcal{A}$ is the acceptance, $\mathcal{B}$ is the branching ratio for J/ψ to decay into electron or muon pairs [26] and N_{Evt} is the number of signal events after background subtraction. N_{Evt} and $\mathcal{A}$ were determined in the signal regions defined for the electron and muon channels in section 5. In the range $40 < W < 140$ GeV and for $Q^2_{min} < Q^2 < 4$ GeV^2 the J/ψ electroproduction cross section is

$$\sigma_{ep\to eJ/\psi p} = 5.37 \pm 0.30(\text{stat.})^{+0.69}_{-0.86}(\text{syst.})^{+0.54}_{-0}(\text{model})\ \text{nb}, \tag{8}$$

using the electron sample and

$$\sigma_{ep\to eJ/\psi p} = 5.04 \pm 0.32(\text{stat.})^{+0.62}_{-0.78}(\text{syst.})^{+0.50}_{-0}(\text{model})\ \text{nb}, \tag{9}$$

using the muon sample. The model error quoted above is due to the difference between the value of the dissociative contribution estimated using EPSOFT and using PYTHIA. In the systematic error we have summed in quadrature all the decay-channel-specific errors and the common systematic errors. The electron and muon cross section results are compatible with each other and with previous measurements in the same W range [4, 12, 13].

9.2 Photoproduction Cross Section

The photoproduction cross section is related to the ep cross section by [28]

$$\sigma_{\gamma p \to J/\psi p} = \frac{\int \Phi(y,Q^2)\sigma_{\gamma p \to J/\psi p}\,(y,Q^2)\,dydQ^2}{\int \Phi(y,Q^2)dydQ^2} = \frac{\sigma_{ep \to eJ/\psi p}}{\Phi_T}, \tag{10}$$

where $\sigma_{\gamma p \to J/\psi p}$ is the mean cross section in a range of W and Φ_T is the effective flux of virtual photons accompanying the positron. The integrals run over the full range of Q^2 and from $y_{min} = W^2_{min}/s$ to $y_{max} = W^2_{max}/s$ where W_{min} and W_{max} are the minimum and maximum values of W respectively. The photoproduction cross section has been determined in four W bins. The results for each of the lepton decay modes and the combined results are reported in table 1. The procedure described in section 9.1 was used to calculate the errors on the cross sections presented in table 1. For the combined results the following procedure was used. The weighted mean cross section was calculated; the weights being obtained by summing the statistical and decay channel specific errors in quadrature. The first error reported on the combined results in table 1 is the error on the weighted mean, the second error is the sum of the common systematic errors added in quadrature. The third error reported on the combined results in table 1 is the systematic error associated with the model of diffraction. The combined results are shown in figure 3 where $\sigma_{\gamma p \to J/\psi p}$ is plotted as a function of W. The points are plotted at the mean values of W reported in table 1. A clear growth of $\sigma_{\gamma p \to J/\psi p}$ with W is observed over the W range covered by this experiment.

The ZEUS data in the range $40 < W < 140$ GeV were fit to the form $\sigma_{\gamma p \to J/\psi p} \propto W^\delta$ with the result $\delta = 0.92 \pm 0.14$ (stat.) ± 0.10 (syst.). The systematic error was obtained as follows. For each source of systematic error in turn the cross sections were displaced from their central values, the fit was performed and the value δ_{si} recorded. The systematic error on δ was taken to be $\sqrt{\sum_i (\delta - \delta_{si})^2}$. The result of the fit is shown in figure 3a. This value of δ disfavours that expected in the Donnachie-Landshoff model [29] (the soft pomeron model) in which δ is expected to take the value $\delta = 0.22$ in this W range. The curve corresponding to the soft pomeron model is shown in figure 3a as a dotted line arbitrarily normalised to the second ZEUS data point.

It is interesting to compare the ratio, $R(\frac{J/\psi}{\rho})$, of the cross section for elastic J/ψ photoproduction to the cross section for elastic ρ production as a function of W. At $W \simeq 12$ GeV $R(\frac{J/\psi}{\rho}) = (1.21 \pm 0.20) \times 10^{-3}$ while at $W \simeq 15$ GeV $R(\frac{J/\psi}{\rho}) = (1.67 \pm 0.23) \times 10^{-3}$ [10, 11, 30]. The results presented in the present paper may be combined with those presented in reference [1] to determine that $R(\frac{J/\psi}{\rho}) = (2.94 \pm 0.74) \times 10^{-3}$ at $W \simeq 70$ GeV showing that $R(\frac{J/\psi}{\rho})$ rises with W. These values are to be compared with $R(\frac{J/\psi}{\rho}) = \frac{8}{9}$ expected on the basis of the quark charges and a flavour independent production mechanism.

The data are replotted in figure 3b together with other measurements of elastic J/ψ photoproduction. The results of two pomeron models [31, 32] are shown in figure 3b. In the model of reference [31] the effective pomeron intercept is assumed to depend upon $\bar{Q}^2_{HKK} = cM_c^2 + Q^2$, where M_c is the mass of the charm quark and the constant $c \approx 1$.

The model of reference [32] assumes a fixed pomeron intercept but includes both a scale dependent pomeron coupling and a mass threshold function. Both models give a good description of the data.

Attempts have been made to describe elastic J/ψ production in perturbative QCD, pQCD. In the approach of Ryskin [22] the pomeron is described as a gluon ladder evaluated in the leading logarithm approximation. In this model the cross section is proportional to $[\alpha_s \bar{x} g(\bar{x}, \bar{q}^2)]^2$, where α_s is the strong coupling constant (assumed fixed and set equal to 0.25) and $\bar{x} g(\bar{x}, \bar{q}^2)$ is the gluon momentum density in the proton. The quantities $\bar{x}$ and $\bar{q}^2$ are given by

$$\bar{x} = \frac{Q^2 + M_{J/\psi}^2 - t}{W^2} \qquad\qquad \bar{q}^2 = \frac{Q^2 + M_{J/\psi}^2 - t}{4} \tag{11}$$

and give the effective momentum fraction and scale at which the gluon density is probed respectively. In the present case both Q^2 and $|t|$ are negligible in comparison to $M_{J/\psi}^2$. For elastic J/ψ photoproduction $\bar{q}^2$ takes a value of approximately 2.5 GeV^2 [22] while the measurements presented here are sensitive to values of $\bar{x}$ in the range $0.4 \times 10^{-3} < \bar{x} < 6 \times 10^{-3}$ [4]. If a gluon distribution of the form $\bar{x} g(\bar{x}, Q^2) \propto \bar{x}^{-\lambda}$ is assumed then the W dependence of $\sigma_{\gamma p \to J/\psi p}$ may be written $\sigma_{\gamma p \to J/\psi p} \propto W^{4\lambda}$. The value of δ reported above gives $\lambda = 0.23 \pm 0.04 \pm 0.03$. This is consistent with our measurement of the gluon distributions based on an analysis of the scaling violations of F_2 extrapolated back to $Q^2 = 2.5$ GeV^2 [33].

Figure 3b shows the results of the pQCD calculation of $\sigma_{\gamma p \to J/\psi p}$ presented in [34] which extends the Ryskin model beyond leading order and includes the effects of the relativistic motion of the c and $\bar{c}$ within the J/ψ and the rescattering of the $c\bar{c}$ pair on the proton. Good agreement with the data is obtained using the MRS-A$'$ [35] parton distributions. Other choices of parton distributions compatible with HERA measurements of F_2 also give an acceptable description of the W dependence of $\sigma_{\gamma p \to J/\psi p}$ over the range $40 < W < 140$ GeV.

9.3 Differential Cross Sections

Figure 4a shows the differential photoproduction cross section $d\sigma/dp_{TJ/\psi}^2$ for the full W range ($40 < W < 140$ GeV). The results from the electron and muon samples have been combined using the procedure described in section 9.2. The contribution from proton dissociative J/ψ production and the Bethe-Heitler process have been subtracted bin by bin. The cross section exhibits the exponential fall characteristic of diffractive processes. A binned likelihood fit to the form

$$\frac{d\sigma}{dp_{TJ/\psi}^2} = A e^{-b_{p_T} p_{TJ/\psi}^2} \tag{12}$$

was performed in which the function in equation 12 was integrated and compared with the measured cross section bin by bin. Fitting over the range $p_{TJ/\psi}^2 < 1$ GeV^2 gives the

result

$$b_{p_T} = 4.3 \pm 0.4^{+0.4}_{-0.6}\ \mathrm{GeV}^{-2}. \tag{13}$$

The differential cross section $d\sigma/d|t|$ may be obtained by dividing $d\sigma/dp^2_{TJ/\psi}$ bin by bin by a factor which corrects for the small Q^2 of the photon. Figure 4b shows the correction factor, F, which is slowly varying and close to 1 for $|t| < 1$ GeV^2. The differential cross section $d\sigma/d|t|$ obtained in this way is plotted in figure 4c. Again, the cross section exhibits an exponential fall and a binned likelihood fit to the form

$$\frac{d\sigma}{d|t|} = Ae^{-b|t|} \tag{14}$$

was performed in which the function in equation 14 was integrated and compared with the measured cross section bin by bin. Fitting over the range $|t| < 1$ GeV^2 gives the result

$$b = 4.6 \pm 0.4^{+0.4}_{-0.6}\ \mathrm{GeV}^{-2}. \tag{15}$$

The systematic error contains the contribution coming from the uncertainty in the correction factor F. The fit for b was repeated for $|t| < 0.8$ GeV^2 and $|t| < 1.2$ GeV^2. The small changes in b obtained are included in the systematic error quoted in equation 15. The size of the statistical and systematic errors on the parameter b prevents us from investigating the dependence of b on W using the data presented here. The slope is in agreement with the result obtained by the H1 collaboration [12, 13] in the same W range. We have previously determined the parameter b in elastic ρ, ω and ϕ photoproduction to be 9.8 ± 0.8 stat. $\pm$ 1.1 syst. GeV^{-2} [1], 10.0 ± 1.2 stat. $\pm$ 1.3 syst. GeV^{-2} [2] and 7.3 ± 1.0 stat. ± 0.8 syst. GeV^{-2} [3] respectively. In geometrical models of vector meson production these results may be interpreted as indicating that the radius of the J/ψ is smaller than that of the ρ, ω and ϕ. When the parameter b is measured in exclusive ρ production in deep inelastic scattering for Q^2 values in the range $7 \lesssim Q^2 \lesssim 25$ GeV^2 a value of $5.1^{+1.2}_{-0.9} \pm 1$ GeV^{-2} is obtained which is significantly smaller than the slope obtained in elastic ρ photoproduction [5]. Thus, in exclusive ρ production b falls as Q^2 is raised from 0 reaching a value of $5.1^{+1.2}_{-}0.9 \pm 1.0$ GeV^{-2} at Q^2 of order 10 GeV^2 comparable to that reported here for J/ψ photoproduction where the hard scale in the scattering process may be set by $M^2_{J/\psi}$.

9.4 Decay Angular Distributions

The J/ψ decay angular distributions can be used to determine elements of the J/ψ spin-density matrix [36]. In the s-channel helicity frame the J/ψ is at rest and the quantisation axis is taken to lie along the J/ψ direction in the photon-proton centre of mass system. The decay angular distribution is a function of θ_h and ϕ_h, the polar and azimuthal angles of the positive lepton in the helicity frame. The angular distributions can be shown to be [37]

$$\frac{1}{N}\frac{dN}{d\cos\theta_h} = \frac{3}{8}\left[1 + r^{04}_{00} + \left(1 - 3r^{04}_{00}\right)\cos^2\theta_h\right], \tag{16}$$

$$\frac{1}{N}\frac{dN}{d\phi_h} = \frac{1}{2\pi}\left[1 + r^{04}_{1-1}\cos 2\phi_h\right]. \tag{17}$$

In the present experiment $Q^2 \approx 0$ GeV^2 so that the J/ψ is expected to be produced predominantly by transverse photons. If s-channel helicity is conserved (SCHC) then the spin density matrix parameters r^{04}_{00} and r^{04}_{1-1} should be close to zero. Under the assumption of SCHC, r^{04}_{00} can be related to the ratio of the photoproduction cross sections for longitudinal and transverse photons

$$R = \frac{1}{\epsilon}\frac{r^{04}_{00}}{1 - r^{04}_{00}} \qquad\qquad \epsilon = \frac{2\,(1-y)}{1 + (1-y)^2 - 2\,(1-y)\,\frac{Q^2_{min}}{Q^2}}, \tag{18}$$

where ϵ is the virtual photon polarisation, i.e. the ratio of the flux of longitudinally polarised photons to the flux of transversely polarised photons. The mean value of ϵ over the kinematic range of Q^2 and y sampled by the present experiment is $\epsilon = 1.043$.

The decay angular distributions are presented in figure 5. No subtraction of the dissociative contribution has been made for the distributions presented in figure 5 since it is assumed that the elastic and dissociative processes have the same angular dependence. The distribution of the polar angle of the positive lepton is shown in figure 5a. A fit has been used to determine r^{04}_{00}. The result $r^{04}_{00} = -0.01 \pm 0.09$ (which gives $R = -0.01 \pm 0.09$) is consistent with SCHC. The distribution of the azimuthal angle of the positive lepton is shown in figure 5b. The distribution is flat and a fit has been made to determine r^{04}_{1-1}. Again, the result $r^{04}_{1-1} = -0.08 \pm 0.07$ is consistent with SCHC.

10 Summary

The cross section for elastic J/ψ photoproduction has been measured using the ZEUS detector at HERA. A significant rise in the cross section with W has been observed for W in the range $40 < W < 140$ GeV. The rise in the cross section with W may be parameterised by $\sigma_{\gamma p \to J/\psi p} \propto W^{\delta}$ with $\delta = 0.92 \pm 0.14(\text{stat.}) \pm 0.10(\text{syst.})$. The measured value of δ is inconsistent with the soft pomeron model. Models based on the vector dominance model plus the exchange of a pomeron can be made to describe the data if the effective pomeron intercept, or the effective pomeron coupling is assumed to depend on the hard scale in the process. QCD based models, which describe the process in terms of the exchange of a gluon ladder evaluated at leading order or beyond leading order, are consistent with the data.

The differential cross section $d\sigma/d|t|$ has been measured and falls exponentially with $|t|$. The slope of the exponential has been measured to be $4.6 \pm 0.4^{+0.4}_{-0.6}$ GeV^{-2} in the range $|t| < 1$ GeV^2. In geometrical models of vector meson production these results may be interpreted as indicating that the radius of the J/ψ is smaller than that of the ρ, ω and ϕ as measured in photoproduction.

The decay angular distributions are consistent with s-channel helicity conservation.

Acknowledgements

We thank the DESY Directorate for their strong support and encouragement. The experiment was made possible by the inventiveness and the diligent efforts of the DESY machine group. The design, construction and installation of the ZEUS detector have been made possible by the ingenuity and dedicated efforts of many people from inside DESY and from the home institutes who are not listed as authors. Their contributions are acknowledged with great appreciation.

References

[1] ZEUS Collab., M. Derrick et al., Z. Phys **C69** (1995) 39.
ZEUS Collab., M. Derrick et al., Z. Phys. **C73** (1997) 253.

[2] ZEUS Collab., M. Derrick et al., Z. Phys. **C73** (1996) 73.

[3] ZEUS Collab., M. Derrick et al., Phys. Lett. **B377** (1996) 259.

[4] ZEUS Collab., M. Derrick et al, Phys. Lett. **B350** (1995) 120.

[5] ZEUS Collab., M. Derrick et al., Phys. Lett. **B356** (1995) 601.

[6] ZEUS Collab., M. Derrick et al., Phys. Lett. **B380** (1996) 220.

[7] ZEUS Collab., M. Derrick et al., Z. Phys. **C69** (1995) 607.
ZEUS Collab., M. Derrick et al., Z. Phys. **C65** (1995) 379.
ZEUS Collab., M. Derrick et al., Phys. Lett. **B316** (1993) 412.

[8] H1 Collab., T. Ahmed et al., Nucl. Phys. **B439** (1995) 471.
H1 Collab., I. Abt et al., Nucl. Phys. **B407** (1993) 515.

[9] B. Knapp et al., Phys. Rev. Lett. **34** (1975) 1040.
U. Camerini et al., Phys. Rev. Lett. **35** (1975) 483.
B. Gittelman et al., Phys. Rev. Lett. **35** (1975) 1616.
T. Nash et al., Phys. Rev. Lett. **36** (1976) 1233.
BFP Collab., A.R. Clark et al., Phys. Rev. Lett. **43** (1979) 187.
EMC Collab., J.J. Aubert et al., Nucl. Phys. **B213** (1983) 1.
NA14 Collab., R. Barate et al., Z. Phys. **C33** (1987) 505.
E687 Collab., P.L. Frabetti et al., Phys. Lett. **B316** (1993) 197.
NMC Collab., M. Arneodo et al., Phys. Lett **B332** (1994) 195.

[10] E401 Collab., M. Binkley et. al., Phys Rev. Lett. **48** (1982) 73.

[11] E516 Collab., B.H. Denby et al., Phys. Rev. Lett. **52** (1984) 795.

[12] H1 Collab., T. Ahmed et al, Phys. Lett. **B338** (1994) 507.

[13] H1 Collab., S. Aid et al, Nucl. Phys. **B472** (1996) 3.

[14] S.D. Holmes et al. Ann. Rev. Nucl. Part. Sci. **35** (1985) 397.

[15] ZEUS Collab., The ZEUS Detector, Status Report, DESY (1993).

[16] C. Alvisi et al., Nucl. Instr. & Meth. **A305** (1991) 30.

[17] N. Harnew et al., Nucl. Instr. & Meth. **A279** (1989) 290.
C.B. Brooks et al., Nucl. Instr. & Meth. **A283** (1989) 477.
B. Foster et al., Nucl. Instr. & Meth. **A338** (1994) 254.

[18] M. Derrick et al., Nucl. Instr. & Meth. **A309** (1991) 77.
A. Andresen et al., Nucl. Instr. & Meth. **A309** (1991) 101.
A. Bernstein et al., Nucl. Instr. & Meth. **A336** (1993) 23.

[19] G. Abbiendi et al., Nucl. Instr & Meth. **A333** (1993) 342.

[20] D. Kisielewska et al., DESY-HERA 85-25 (1985),
J. Andruszków et al., DESY-92-066 (1992).

[21] M. Arneodo, L. Lamberti and M.G. Ryskin, Comp. Phys. Comm. 100 (1997) 195.

[22] M.G. Ryskin, Z. Phys **C57** (1993) 89.

[23] S.P. Baranov et al., Proc. of the Workshop 'Physics at HERA', Vol. III, Oct. 1991, 1478.

[24] J.A.M. Vermaseren, Nucl.Phys., **B229** (1983) 347.

[25] T. Sjöstrand and M. Bengtsson, Comp. Phys. Comm. **43** (1987) 367.
M. Bengtsson and T. Sjöstrand, Comp. Phys. Comm. **46** (1987) 43.
T. Sjöstrand, Proc. of the Workshop 'Physics at HERA', Vol. III, Oct. 1991, 1405.

[26] Particle Data Group, R.M. Barnett et al., Phys. Rev. **D54** (1996) 1.

[27] CDF Collab., F. Abe et al., Phys. Rev. **D50** (1994) 5535.

[28] V.N. Gribov et al., Sov. Phys. JETP **14** (1962) 1308.
V.M. Budnev et al., Phys. Rep. **15C** (1975) 181.

[29] A. Donnachie and P.V. Landshoff, Phys. Lett. **B348** (1995) 213.

[30] R.M. Egloff et al., Phys. Rev. Lett. **43** (1979) 657.

[31] L.P.A. Haakman, A. Kaidalov, J.H. Koch, Phys. Lett. **B365** (1996) 411.

[32] L.L. Jenkovszky, E.S. Martynov and F. Paccanoni, Novy Svet Hadrons (1996) 170.

[33] ZEUS Collaboration, M. Derrick et al., Phys. Lett. **B345** (1995) 576.

[34] M.G. Ryskin, R.G. Roberts, A.D. Martin, E.M. Levin, RAL-TR-95-065.

[35] A.D. Martin, W.J. Stirling, R.G. Roberts, Phys. Lett. **B354** (1995) 155.

[36] K. Schilling et al., Nucl. Phys **B15** (1970) 397.
K. Schilling and G. Wolf, Nucl. Phys. **B61** (1973) 381.

[37] B. Humpert and A.C.D. Wright, Phys. Let. **B65** (1976) 463.
B. Humpert and A.C.D. Wright, Phys. Rev. **D15** (1977) 2503.

[38] J.J. Sakurai, Phys. Rev. Lett. **22** (1969) 981.

W Range (GeV)	Mode	N_{Sig}	$\mathcal{A}$	$\sigma_{ep\to eJ/\psi p}$ (nb)	Φ_T	$\sigma_{\gamma p\to J/\psi p}$ (nb)	$\sigma_{\gamma p\to J/\psi p}$ (nb) combined
40-60 $\langle W\rangle = 49.8 \pm 0.8$	e^+e^-	84 ± 10	0.28	$1.23 \pm 0.14^{+0.17\ +0.12}_{-0.21\ -\ 0}$	0.0411	$29.9 \pm 3.4^{+\ 4.1\ +\ 2.9}_{-\ 5.1\ -\ 0}$	$30.4 \pm 3.4^{+2.9\ +\ 3.2}_{-4.4\ -\ 0}$
	$\mu^+\mu^-$	$48 \pm\ 7$	0.23	$1.28 \pm 0.19^{+0.15\ +0.13}_{-0.22\ -\ 0}$	0.0411	$31.1 \pm 4.6^{+3.6\ +\ 3.2}_{-5.4\ -\ 0}$	
60-80 $\langle W\rangle = 71.2 \pm 0.7$	e^+e^-	98 ± 11	0.33	$1.24 \pm 0.13^{+0.16\ +0.12}_{-0.20\ -\ 0}$	0.0266	$46.6 \pm 4.9^{+\ 6.0\ +\ 4.5}_{-\ 7.5\ -\ 0}$	$42.9 \pm 4.5^{+4.1\ +\ 4.1}_{-5.6\ -\ 0}$
	$\mu^+\mu^-$	$61 \pm\ 8$	0.35	$1.05 \pm 0.14^{+0.13\ +0.11}_{-0.16\ -\ 0}$	0.0266	$39.5 \pm 5.3^{+4.9\ +\ 4.1}_{-6.0\ -\ 0}$	
80-100 $\langle W\rangle = 89.6 \pm 0.7$	e^+e^-	92 ± 10	0.32	$1.19 \pm 0.13^{+0.15\ +0.12}_{-0.18\ -\ 0}$	0.0189	$63.0 \pm 6.9^{+\ 7.9\ +6.3}_{-9.5\ -\ 0}$	$57.7 \pm 5.8^{+5.3\ +5.8}_{-6.9\ -\ 0}$
	$\mu^+\mu^-$	$70 \pm\ 9$	0.42	$1.01 \pm 0.12^{+0.14\ +0.10}_{-0.14\ -\ 0}$	0.0189	$53.4 \pm 6.3^{+7.4\ +\ 5.3}_{-7.4\ -\ 0}$	
100-140 $\langle W\rangle = 121 \pm 1$	e^+e^-	$81 \pm\ 9$	0.21	$1.59 \pm 0.18^{+0.24\ +0.16}_{-0.27\ -\ 0}$	0.0251	$63.3 \pm 7.2^{+9.6\ +\ 6.4}_{-10.8\ -\ 0}$	$66.5 \pm 6.8^{+6.4\ +6.8}_{-9.6\ -\ 0}$
	$\mu^+\mu^-$	87 ± 10	0.30	$1.74 \pm 0.20^{+0.23\ +0.17}_{-0.28\ -\ 0}$	0.0251	$69.3 \pm 8.0^{+9.2\ +6.8}_{-11.2\ -\ 0}$	

Table 1: The results for the integrated J/ψ photoproduction cross section as a function of W. N_{Sig} is the number of events after subtraction of the Bethe-Heitler contribution and $\mathcal{A}$ is the acceptance. The photon flux Φ_T is calculated as described in the text and used to calculate the γp cross section, $\sigma_{\gamma p\to J/\psi p}$, from the ep cross section, $\sigma_{ep\to eJ/\psi p}$. Cross sections for the individual channels are quoted with the first error being statistical and the second systematic. The third error is the error attributed to the model of proton dissociation used for background subtraction and is described in the text. The combined electron and muon results have been obtained by averaging as described in the text. Here the first error contains the combined statistical and decay channel specific errors while the second contains all sources of common systematic error. The error attributed to the model of proton dissociation is the third error.

Breakdown of Contributions to the Systematic Error								
Values are quoted in percent								
Decay Channel Specific Systematic Errors								
	Electron Channel				Muon Channel			
W bin (GeV)	40-60	60-80	80-100	100-140	40-60	60-80	80-100	100-140
Trigger	$^{+7}_{-7}$	$^{+7}_{-7}$	$^{+7}_{-7}$	$^{+7}_{-7}$	$^{+5}_{-5}$	$^{+5}_{-5}$	$^{+5}_{-5}$	$^{+5}_{-5}$
Event selection	$^{+5.7}_{-4.6}$	$^{+4.6}_{-4.9}$	$^{+3.0}_{-4.0}$	$^{+8.8}_{-3.8}$	$^{+2.0}_{-6.3}$	$^{+5.6}_{-4.1}$	$^{+7.1}_{-0.0}$	$^{+7.0}_{-2.0}$
Pion misidentification	$^{+0}_{-1.5}$	$^{+0}_{-1.5}$	$^{+0}_{-1.5}$	$^{+0}_{-1.5}$				
Muon chamber efficiency					$^{+2}_{-2}$	$^{+2}_{-2}$	$^{+2}_{-2}$	$^{+2}_{-2}$
Branching ratio	$^{+3.2}_{-3.2}$	$^{+3.2}_{-3.2}$	$^{+3.2}_{-3.2}$	$^{+3.2}_{-3.2}$	$^{+3.2}_{-3.2}$	$^{+3.2}_{-3.2}$	$^{+3.2}_{-3.2}$	$^{+3.2}_{-3.2}$
Subtotal	$^{+9.6}_{-9.1}$	$^{+9.0}_{-9.2}$	$^{+8.3}_{-8.8}$	$^{+11.7}_{-8.7}$	$^{+6.6}_{-8.9}$	$^{+8.4}_{-7.5}$	$^{+9.5}_{-6.3}$	$^{+9.4}_{-6.6}$
Common Systematic Errors								
W bin (GeV)	40-60		60-80		80-100		100-140	
Acceptance	$^{+3}_{-3}$							
Elastic definition	$^{+1}_{-3}$							
Radiative corrections	$^{+4}_{-4}$							
Helicity distribution	$^{+0}_{-10}$		$^{+0}_{-8}$		$^{+0}_{-6}$		$^{+0}_{-10}$	
Proton dissociation	$^{+6}_{-7}$							
Model of dissociation	$^{+10}_{-0}$							
ψ' contamination	$^{+1}_{-1}$							
Luminosity	$^{+1.5}_{-1.5}$							
Total Systematic Errors								
	Electron Channel				Muon Channel			
W bin (GeV)	40-60	60-80	80-100	100-140	40-60	60-80	80-100	100-140
Total	$^{+16.0}_{-16.4}$	$^{+15.7}_{-15.3}$	$^{+15.3}_{-14.1}$	$^{+17.4}_{-16.2}$	$^{+14.5}_{-16.3}$	$^{+15.4}_{-14.4}$	$^{+16.0}_{-12.7}$	$^{+15.9}_{-15.2}$

Table 2: The contributions to the systematic errors on the J/ψ photoproduction cross section. The contributions to the systematic error are divided into *Decay Channel Specific Systematic Errors* and *Common Systematic Errors* as described in section 8.

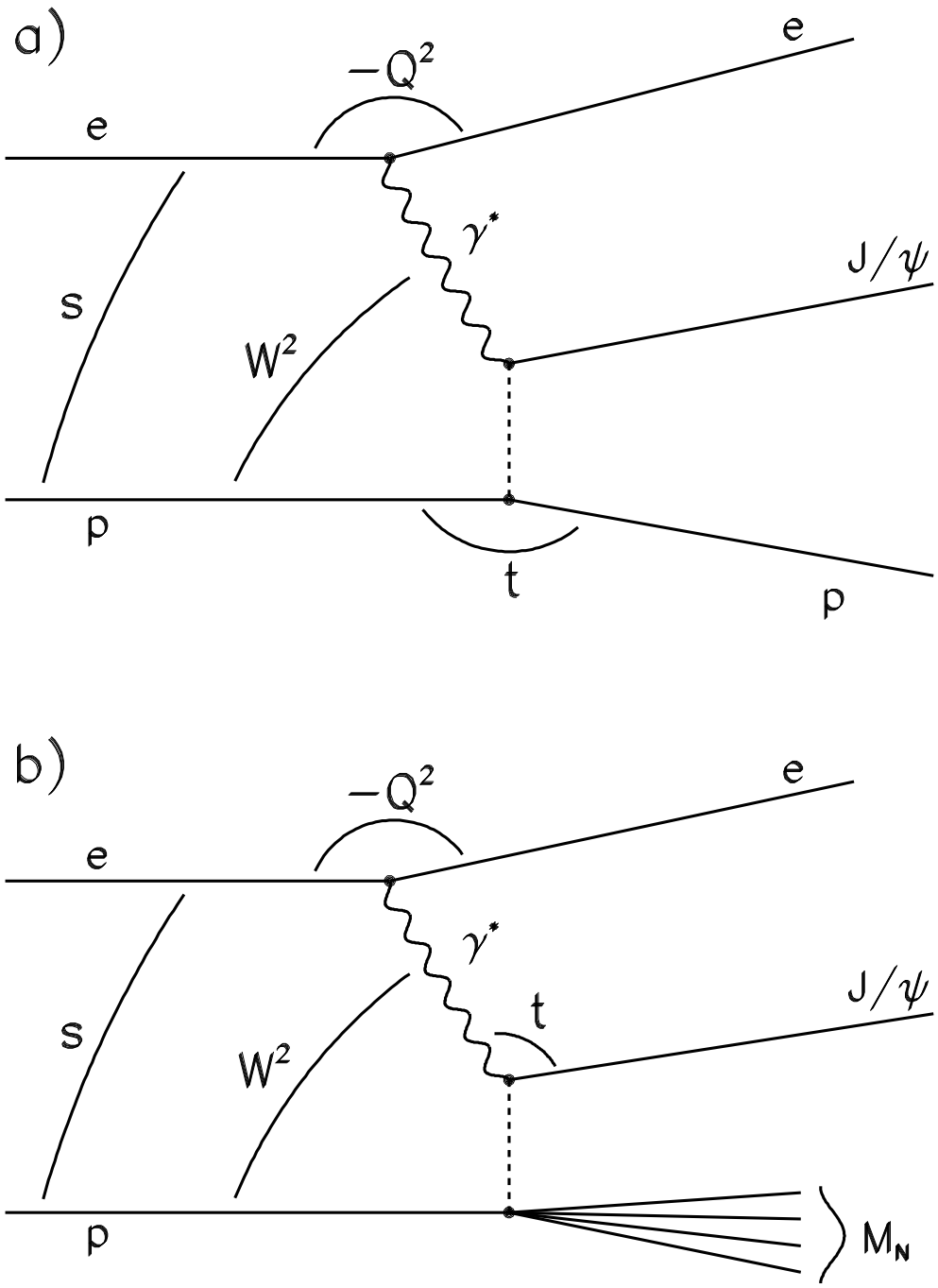

Figure 1: Schematic diagrams for diffractive J/ψ electroproduction. (a) The mechanism for elastic vector meson production. (b) Proton dissociative J/ψ photoproduction where the proton dissociates into a hadronic system of invariant mass M_N.

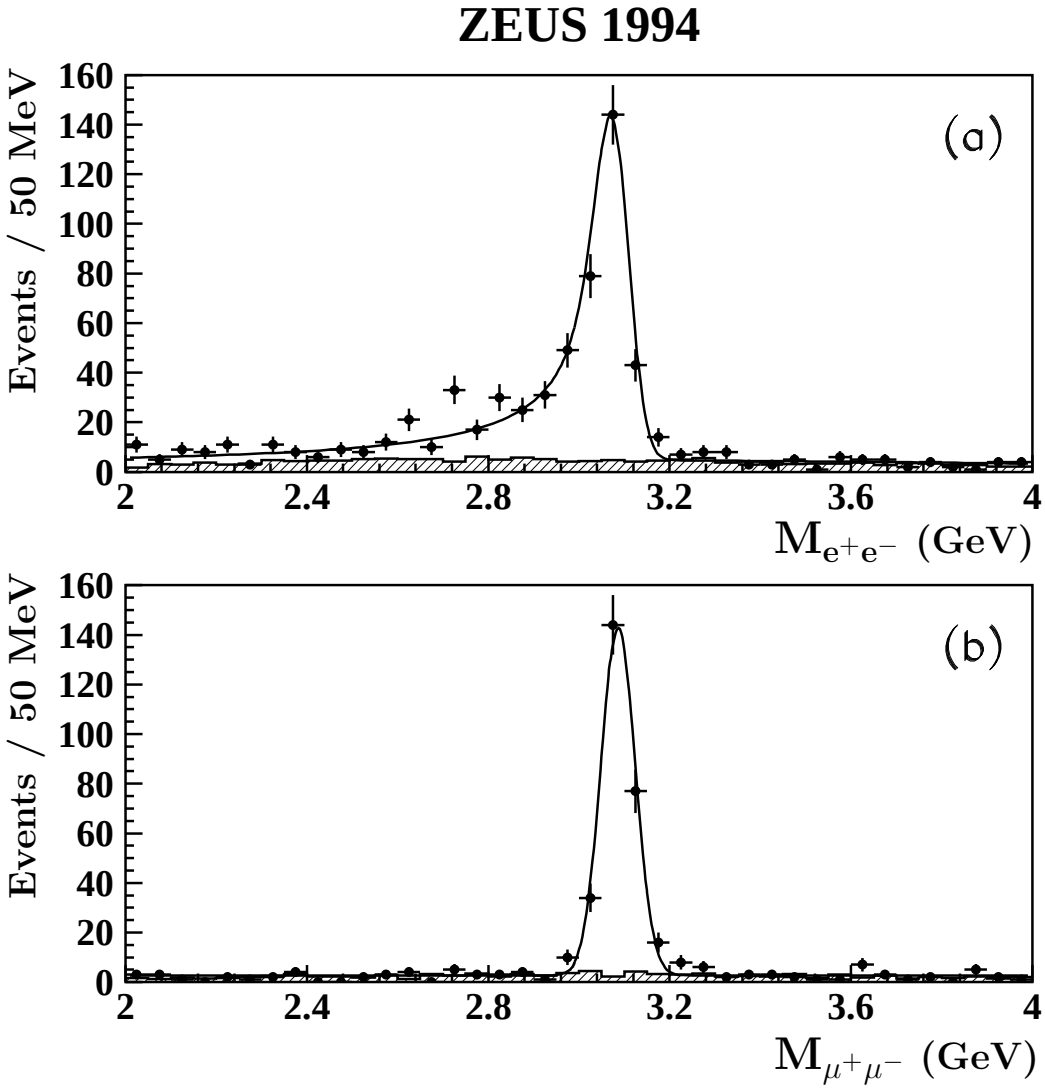

Figure 2: (a) The mass distribution of the events in the electron pair sample. A clear peak at the J/ψ mass is observed. The solid line shows the result of a fit in which a Gaussian resolution function has been convoluted with a radiative J/ψ mass spectrum and added to a polynomial background. (b) The mass distribution for events in the muon pair sample. The solid line shows the result of a fit in which a Gaussian resolution function has been added to a flat background function. For both the electron and muon channels the contribution of events from the Bethe-Heitler process is shown as the hatched area.

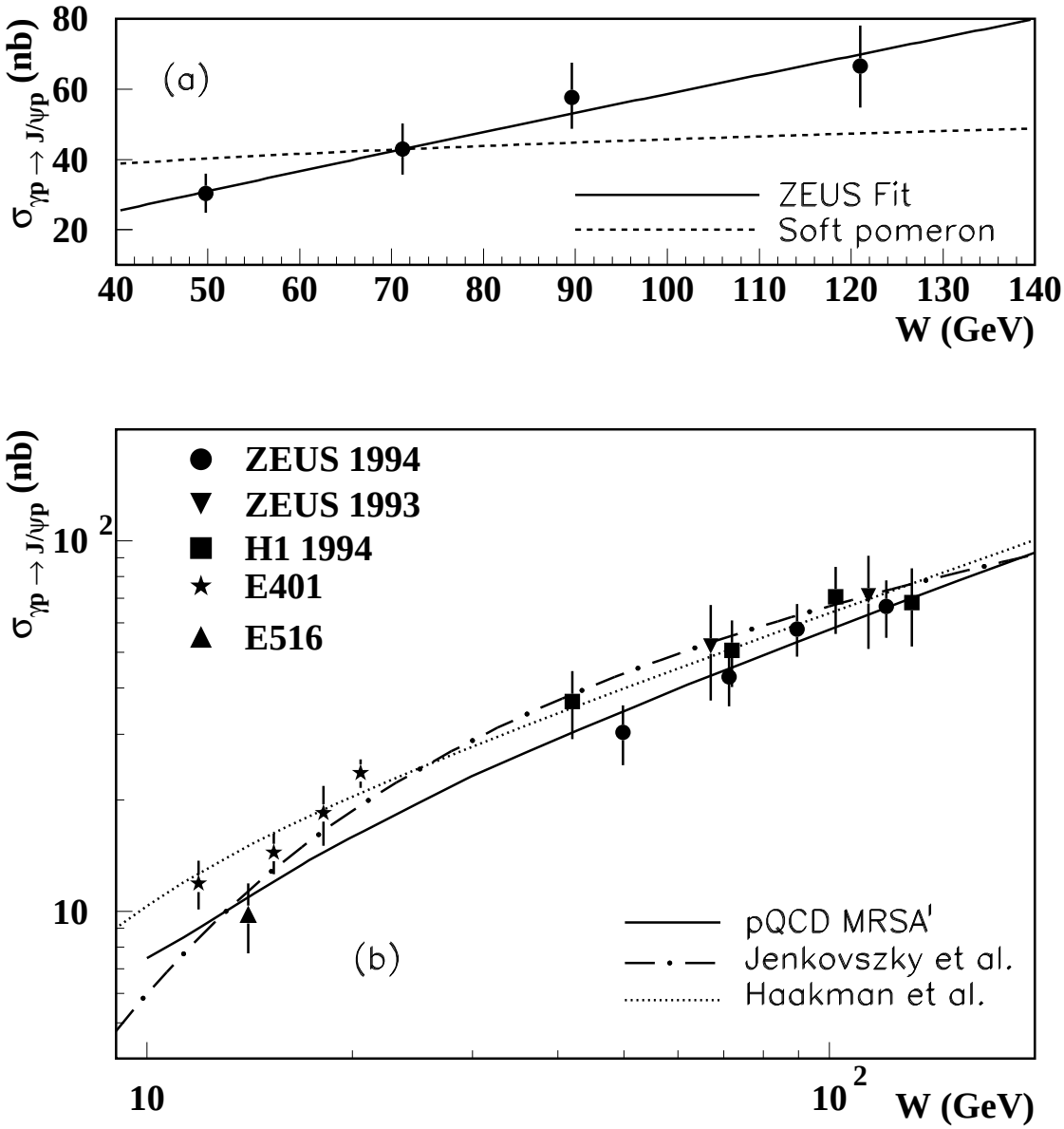

Figure 3: The elastic J/ψ photoproduction cross section as a function of W. (a) Shows the results of this analysis. The error bars represent the statistical and systematic errors added in quadrature. The solid line shows the result of the fit to the data using the expression $\sigma_{\gamma p \to J/\psi p} \propto W^{\delta}$. As described in the text the value $\delta = 0.92 \pm 0.14 \pm 0.10$ was obtained. The dashed line shows the prediction of a soft pomeron model [29] in which $\delta \approx 0.22$. (b) The results of this analysis (solid circles) are compared to data from H1, ZEUS and the results of lower energy measurements [9, 10]. The result of a pQCD calculation [34] in which the MRS-A$'$ [35] parton distributions have been used is shown as the solid line. The result of the calculation presented in [31] is shown by the dotted line. The result of the calculation presented in [32] is shown by the long dash dotted line.

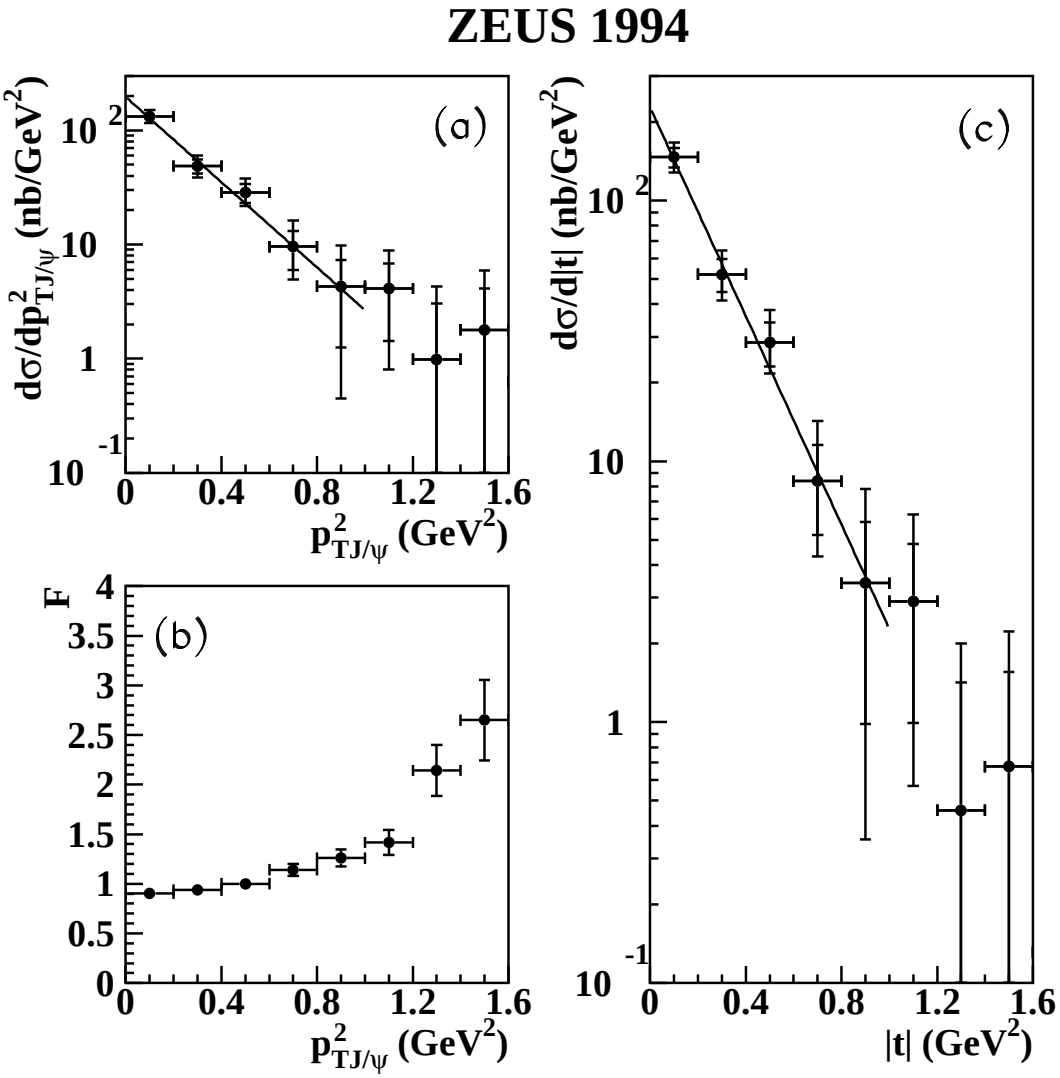

Figure 4: The distribution of transverse momentum squared for J/ψ produced in the reaction $\gamma p \to J/\psi p$ in the kinematic range $40 < W < 140$ GeV. (a) The differential cross section $d\sigma/dp^2_{TJ/\psi}$. The data are shown as the points and the result of the exponential fit in the range $p^2_T < 1$ GeV^2 is shown as the solid line. (b) The correction factor, F, required to obtain the $|t|$ distribution from the $p^2_{TJ/\psi}$ distribution by accounting for the Q^2 of the photon. (c) The differential cross section $d\sigma/d|t|$. The result of the exponential fit in the range $|t| < 1$ GeV^2 is shown as the solid line. In (a) and (c) the inner error bars represent the statistical and decay-channel-specific errors added in quadrature, the outer ones statistical, decay-channel-specific errors and common systematic errors added in quadrature.

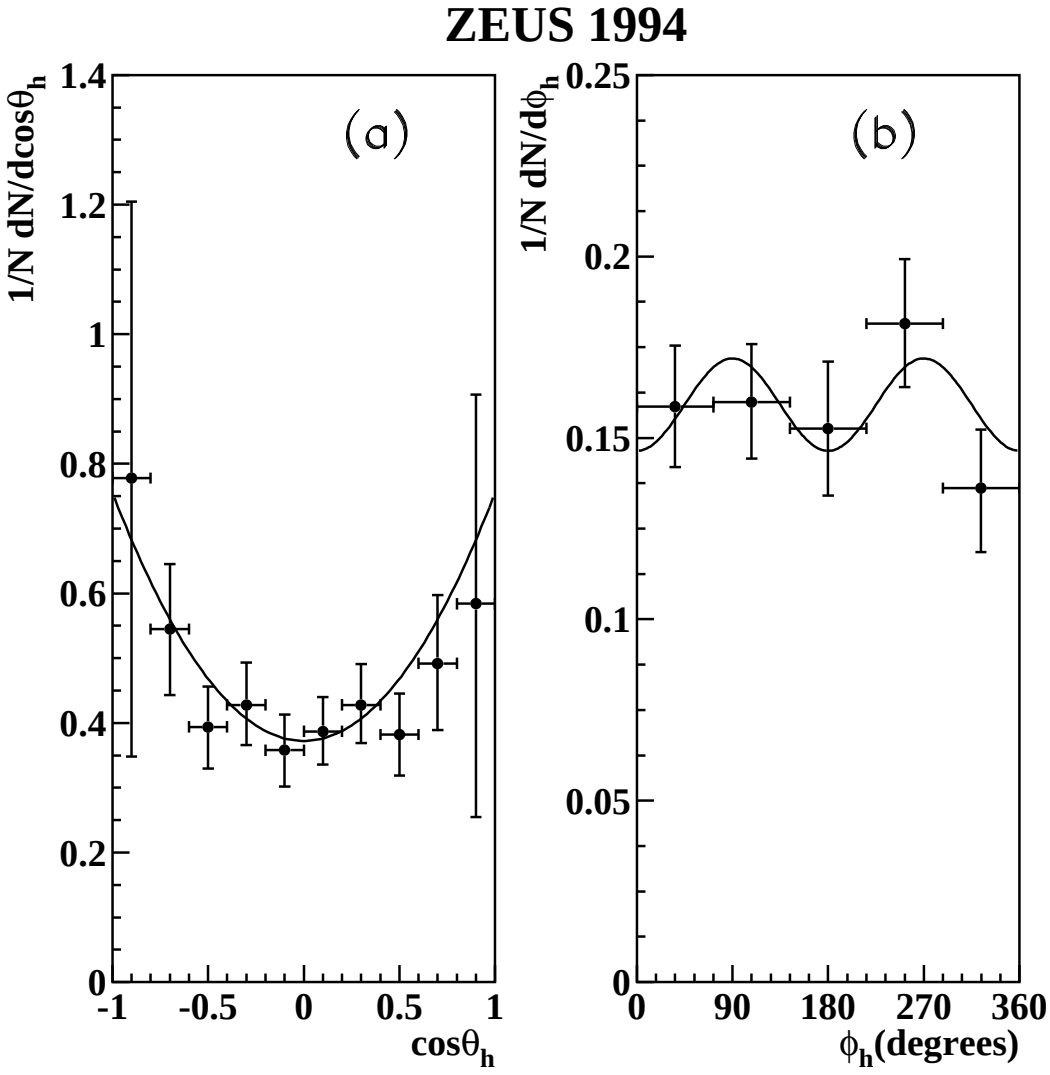

Figure 5: Acceptance corrected decay angular distributions for the J/ψ in the reaction $ep \to eJ/\psi p$ in the kinematic range $40 < W < 140$ GeV. No subtraction of the proton dissociative contribution to the sample has been made for the data presented in this figure since the angular dependence of the proton dissociative and elastic J/ψ production is assumed to be the same. The curves are the results of the fits described in the text. The error bars represent the statistical, decay-channel-specific errors and common systematic errors added in quadrature.